Supplementary Material

One-dimensional iron(II) compounds exhibiting spin crossover and liquid crystalline properties in the room temperature region

M. Seredyuk[a], A. B. Gaspar[b]*, V. Ksenofontov[a], Y. Galyametdinov[c], M. Verdaguer[d], F. Villain[d], P. Gütlich[a]*

STable 1. TGA and IR data for compounds **C*n*-1** and **C*n*-3**.

Compound	TGA, w/w [%] (*T*) [a]	IR/cm^{-1} [b]						
		ν(C–H$_{trz}$)	ν_s(CH$_2$), ν_{as}(CH$_2$)	ν(C=O)	δ(CH$_2$)	ρ(CH$_2$)	τ_2	ν(Anion)
C$_4$-1	0.9 (322 K)	3104	2936	1700	1466	720	624	1253, 1169, 1030
C$_6$-1	1.2 (320 K)	3102	2932, 2859	1700	1464	723	627	1256, 1169, 1030
C$_8$-1	0.8 (327 K)	3101	2927, 2856	1700	1466	723	628	1255, 1168, 1029
C$_{10}$-1	0.3 (324 K)	3110	2925, 2854	1701	1466	721	626	1256, 1169, 1029
C$_{12}$-1	0.3 (320 K)	3110	2924, 2853	1700	1469	721	625	1257, 1169, 1029
C$_4$-3	1.6 (324 K)	3124	2935	1699	1466	720	627	1092, 1070, 1051
C$_6$-3	1.7 (320 K)	3126	2934, 2861	1701	1458	725	626	1093, 1060
C$_8$-3	1.4 (320 K)	3126	2927, 2856	1703	1469	723	624	1093, 1060
C$_{10}$-3	0.9 (320 K)	3125	2925, 2854	1705	1465	721	623	1089, 1059
C$_{12}$-3	0.6 (320 K)	3125	2924, 2853	1704	1465	721	624	1082, 1059

[a] Value is given at the point where the plateau is reached. *T* is the temperature at which the dehydration process is centered; [b] ν, stretching; δ, bending; ρ, rocking; τ, ring torsion vibration; as, asymmetric, s, symmetric.

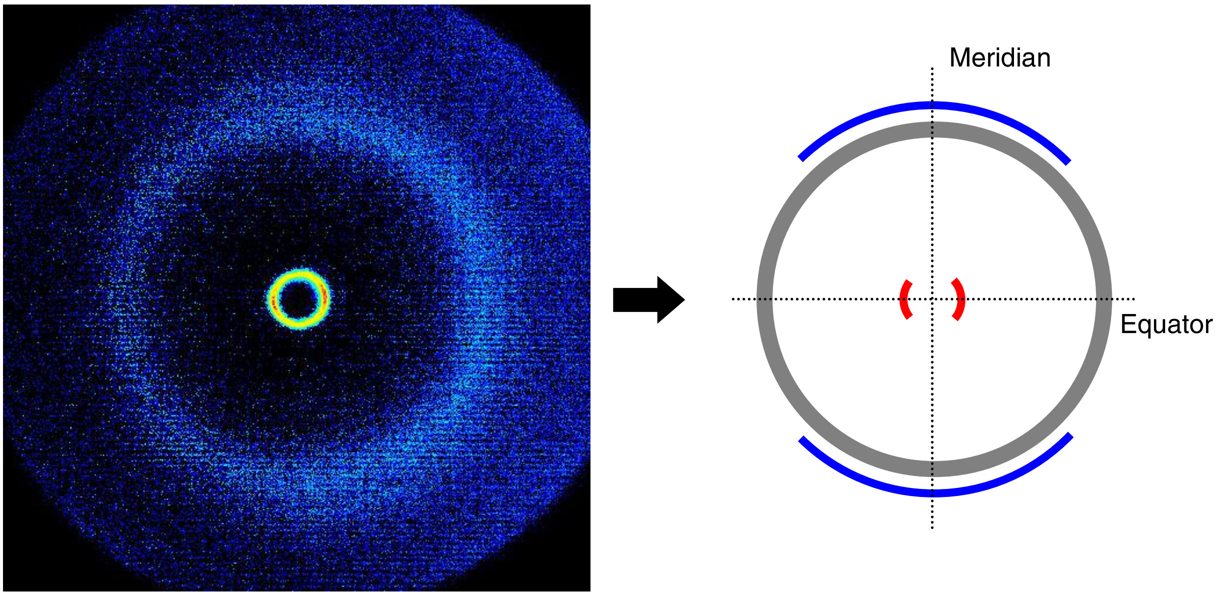

SFigure 1. 2D-WAXS pattern from the oriented sample of $\mathbf{C_{12}}$**-1** ($\mathbf{C_{12}}$**-2**) at 370 K. A relatively sharp pair of equatorial reflections in the low-angle regime originates from the intercolumnar ordering, whereas a pair of weak meridional reflections is due to intracolumnar ordering of Fe(II) ions. The diffuse circular reflection is attributable to the liquid-like alkyl chains.

SFigure 2. DSC profiles in heating and cooling modes for: a) **C_4-1**, **C_4-2** ; b) **C_6-1**, **C_6-2**; c) **C_8-1**, **C_8-2**; d) **C_{10}-1**, **C_{10}-2**; e) **C_{12}-1**, **C_{12}-2**; f) **C_4-3**, **C_4-4**; g) **C_6-3**, **C_6-4**; h) **C_8-3**, **C_8-4**; i) **C_{10}-3**, **C_{10}-4**; j) **C_{12}-3**, **C_{12}-4**. Arrows show direction of scanning runs.

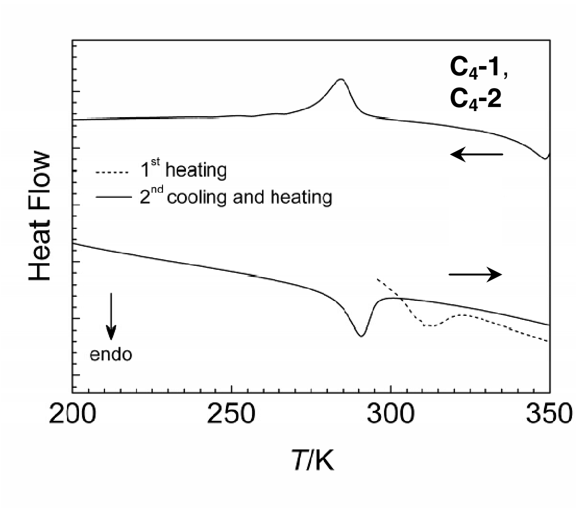

a

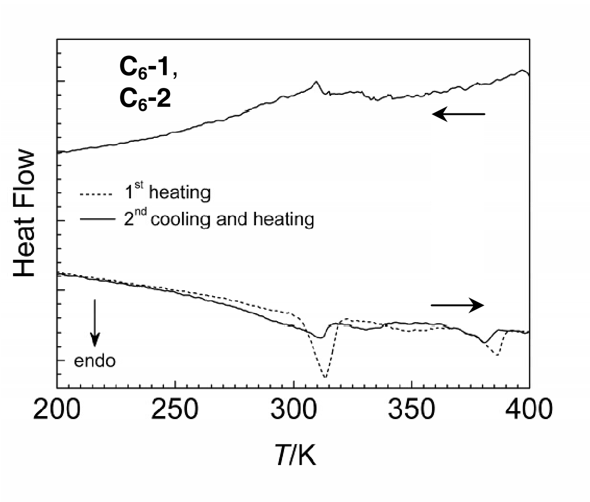

b

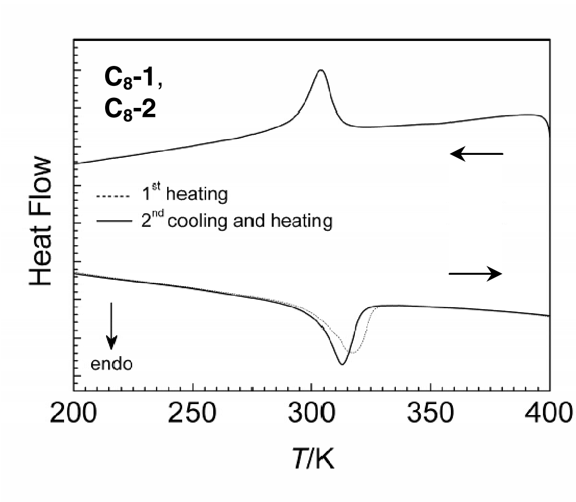

c

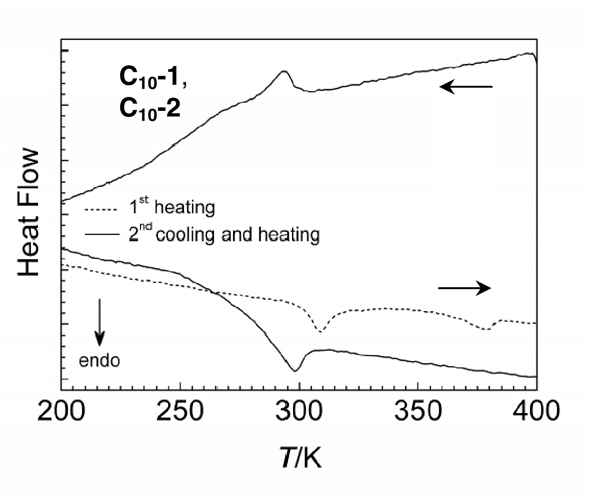

d

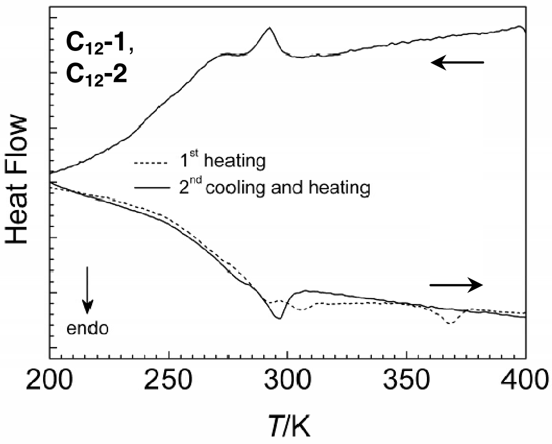

C_{12}-1,
C_{12}-2
1st heating
2nd cooling and heating
Heat Flow
endo
200
250
300
350
400
T/K

e

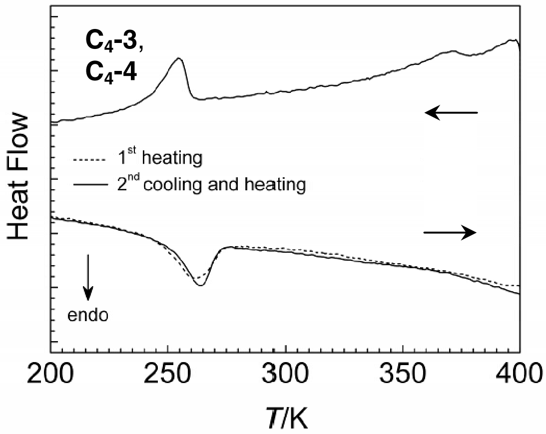

C_4-3,
C_4-4
1st heating
2nd cooling and heating
Heat Flow
endo
200
250
300
350
400
T/K

f

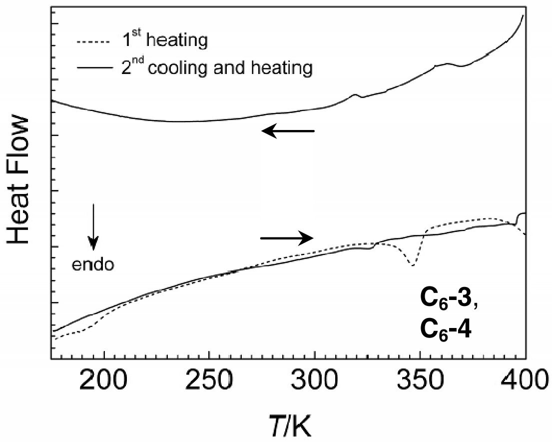

1st heating
2nd cooling and heating
Heat Flow
endo
C_6-3,
C_6-4
200
250
300
350
400
T/K

g

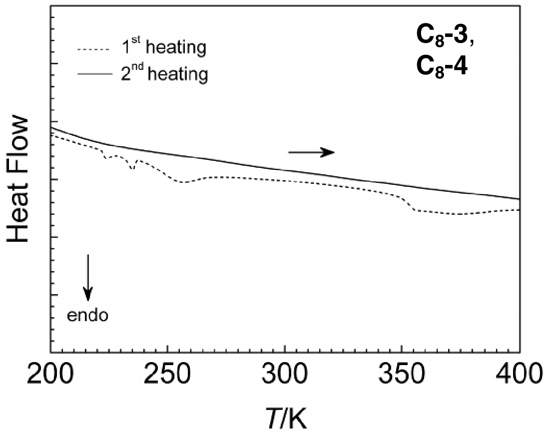

1st heating
2nd heating
C_8-3,
C_8-4
Heat Flow
endo
200
250
300
350
400
T/K

h

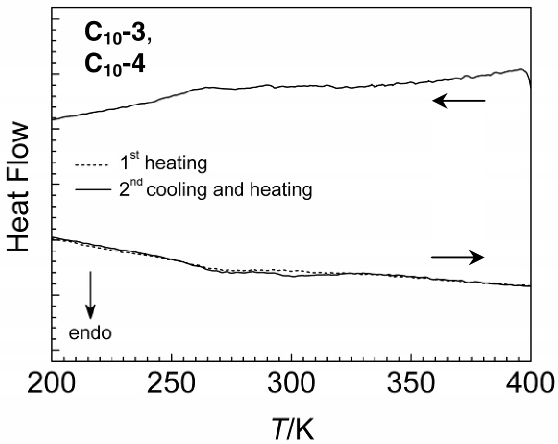

C_{10}-3,
C_{10}-4
1st heating
2nd cooling and heating
Heat Flow
endo
200
250
300
350
400
T/K

i

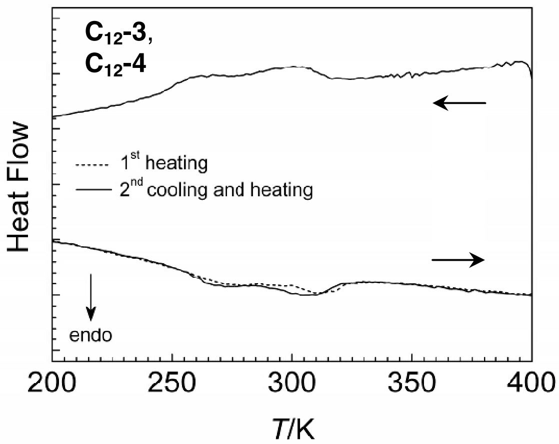

C_{12}-3,
C_{12}-4
1st heating
2nd cooling and heating
Heat Flow
endo
200
250
300
350
400
T/K

j

SFigure 3. Mössbauer spectra of: a) **C_4-1** at 250 and 340 K; b) **C_6-1** at 4.2 K; c) **C_8-1** at 4.2 K; d) **C_{10}-1** at 120 K; e) **C_{12}-1** at 4.2 K; f) **C_4-3** at 200 and 300 K; g) **C_6-3** at 4.2 and 250 K; h) **C_8-3** at 80 K; i) **C_{10}-3** at 80 K; j) **C_{12}-3** and k) **C_{12}-4** at 80 K.

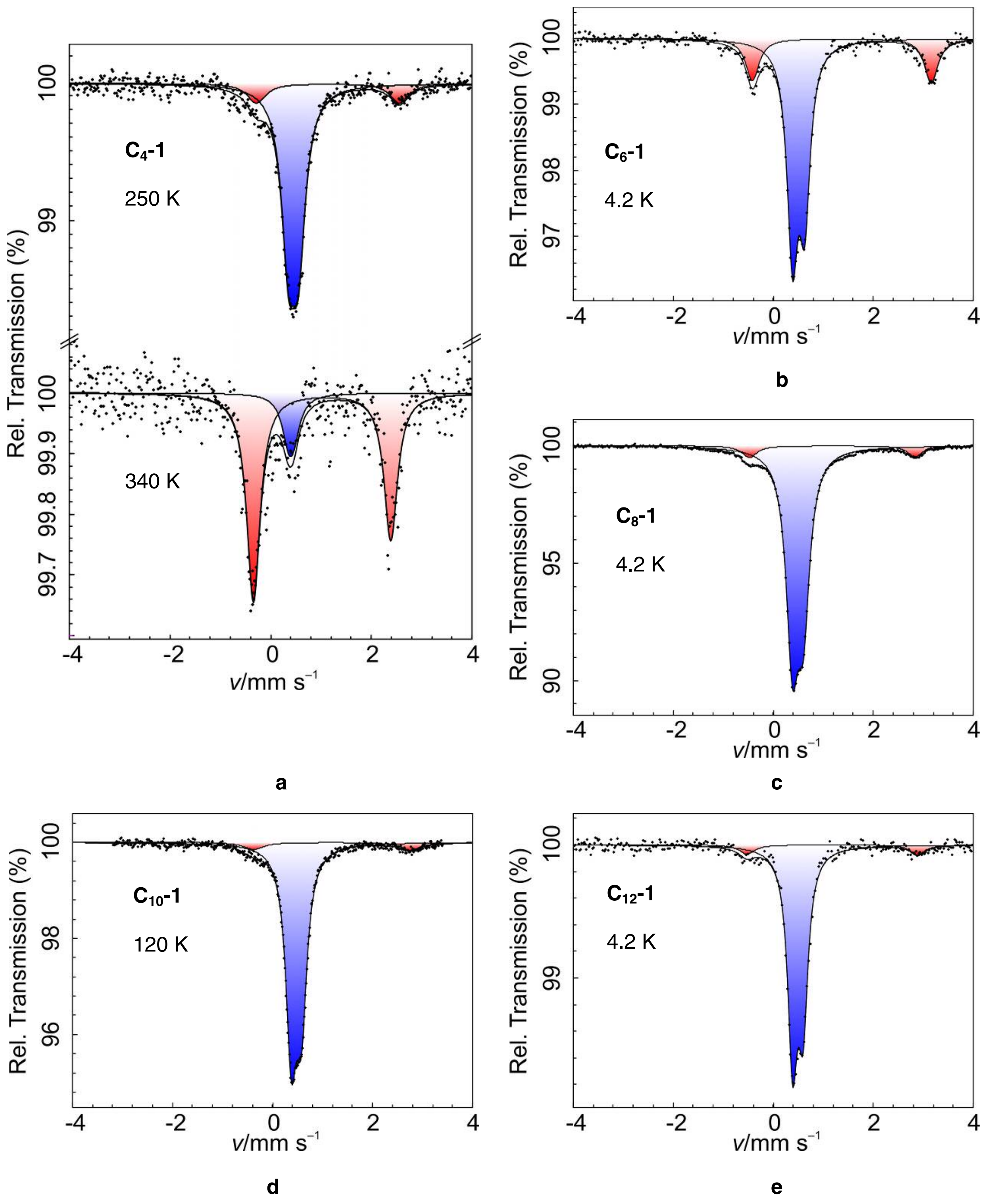

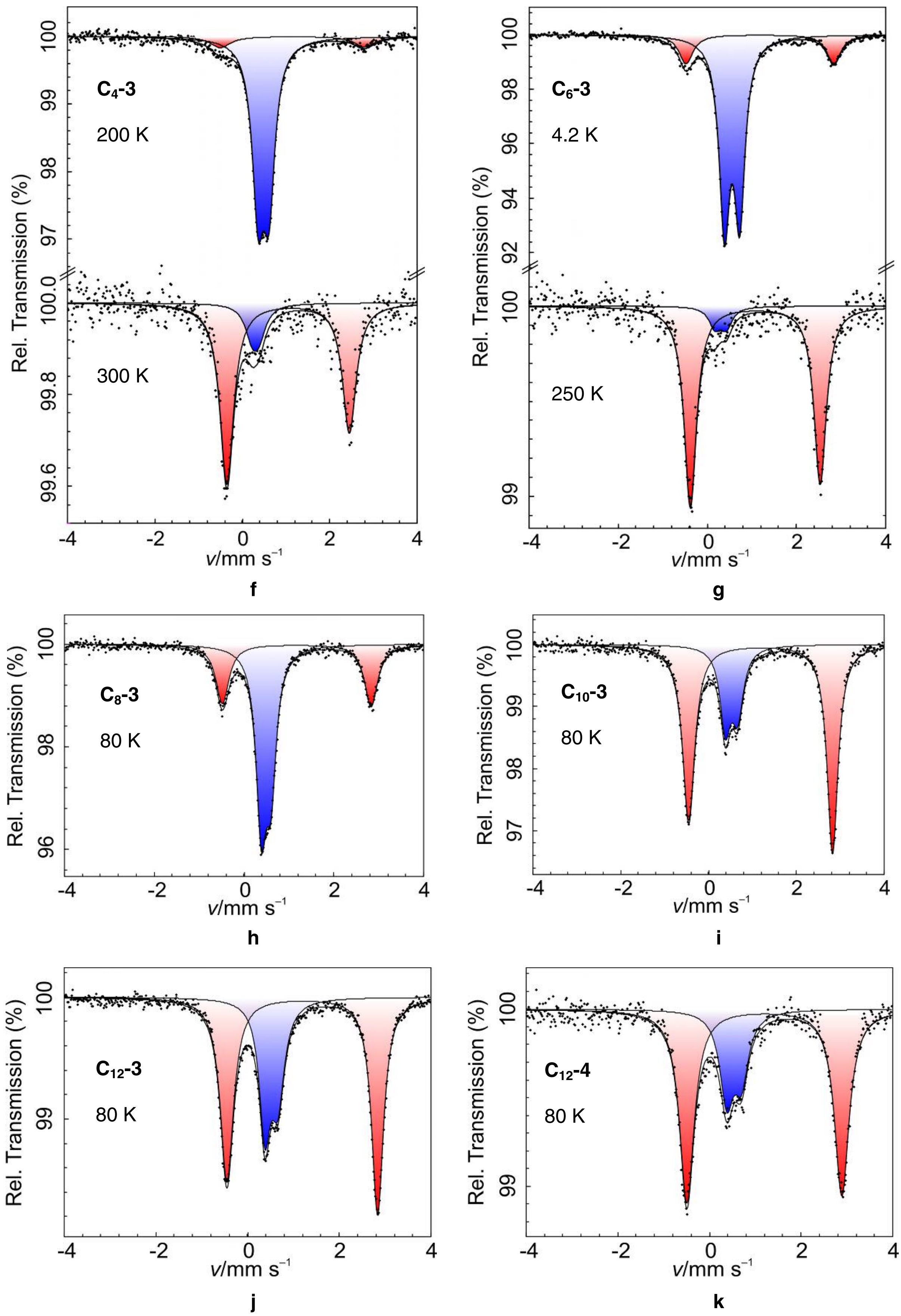
C4-3
200 K
300 K
Rel. Transmission (%)
v/mm s−1
f
C6-3
4.2 K
250 K
Rel. Transmission (%)
v/mm s−1
g
C8-3
80 K
Rel. Transmission (%)
v/mm s−1
h
C10-3
80 K
Rel. Transmission (%)
v/mm s−1
i
C12-3
80 K
Rel. Transmission (%)
v/mm s−1
j
C12-4
80 K
Rel. Transmission (%)
v/mm s−1
k

STable 2. Mössbauer parameters, isomer shift (δ, relative to α-iron), quadrupole splitting (ΔE_Q), half-width of the lines ($\Gamma_{1/2}$) and percentage of populations in the HS and LS states at different temperatures (A) for **C*n*-1**, **C*n*-3** (n = 4, 6, 8, 10, 12) and **C_{12}-4**.

Compound	*T*/K	Spin state	*δ*/mm s^{-1}	Δ*E*$_Q$/mm s^{-1}	*Γ*$_{1/2}$/mm s^{-1}	*A*/%
C_4-1	80	LS	0.50(0)	0.21(0)	0.17(1)	94.4(10)
		HS	1.11(0)	3.18(1)	*0.17*	5.6(8)
	250	LS	0.45(1)	0.20(1)	0.17(0)	87.3(17)
		HS	1.15(1)	2.81(0)	*0.17*	12.7(22)
	340	LS	0.32(6)	0.27(0)	0.16(0)	17.4(40)
		HS	1.02(1)	2.73(2)	*0.16*	82.6(54)
C_6-1	4.2	LS	0.51(1)	0.24(0)	0.13(5)	77.5(17)
		HS	1.37(1)	3.58(2)	0.16(2)	22.5(24)
C_8-1	4.2	LS	0.49(1)	0.22(0)	0.15(0)	92.6(4)
		HS	1.18(1)	3.30(2)	*0.18*	7.4(4)
C_{10}-1	120	LS	0.48(2)	0.20(0)	0.13(0)	92.5(8)
		HS	1.21(2)	3.10(5)	*0.14*	7.5(18)
C_{12}-1	4.2	LS	0.49(0)	0.20(1)	0.12(0)	92.3(21)
		HS	1.18(0)	3.42(2)	0.19(0)	7.7(35)
C_4-3	80	LS	0.51(0)	0.25(0)	0.16(1)	91.2(4)
		HS	1.17(1)	3.45(2)	0.21(1)	8.8(6)
	200	LS	0.49(1)	0.25(1)	0.17(1)	92.4(2)
		HS	1.14(3)	3.29(6)	*0.16*	7.6(1)
	300	LS	0.35(1)	*0.2*	*0.22*	16.8(29)
		HS	1.05(1)	2.80(2)	0.19(1)	83.2(59)
C_6-3	4.2	LS	0.55(0)	0.34(0)	0.14(0)	82.1(84)
		HS	1.18(1)	3.32(2)	0.19(1)	17.9(13)
	80	LS	0.55(0)	0.35(0)	0.15(0)	69.4(11)
		HS	1.17(0)	3.27(1)	0.17(1)	30.6(16)
	190	LS	0.51(1)	0.33(1)	0.18(1)	23.9(15)
		HS	1.11(0)	3.13(0)	0.17(1)	76.1(20)
	250	LS	0.32(0)	0.26(1)	*0.16*	8.3(25)
		HS	1.08(0)	2.91(0)	0.17(0)	91.7(50)
C_8-3	80	LS	0.49(0)	0.22(1)	0.14(3)	65.8(9)
		HS	1.17(0)	3.31(0)	0.18(1)	34.2(14)
C_{10}-3	80	LS	0.52(0)	0.28(1)	0.16(2)	26.5(9)
		HS	1.19(1)	3.28(0)	0.15(0)	73.5(13)
C_{12}-3	80	LS	0.52(1)	0.28(1)	0.18(1)	34.7(7)
		HS	1.19(0)	3.28(0)	0.16(1)	65.3(10)
C_{12}-4	80	LS	0.54(1)	0.32(0)	0.19(1)	27.6(18)
		HS	1.20(1)	3.38(0)	0.19(0)	72.4(25)

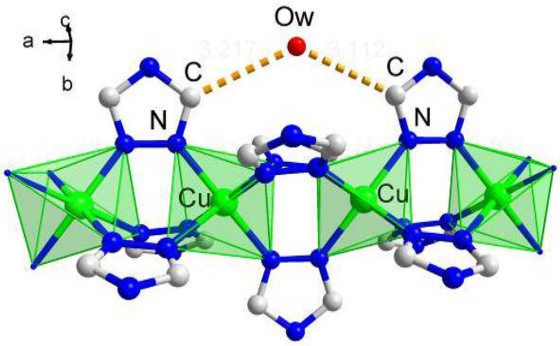

a

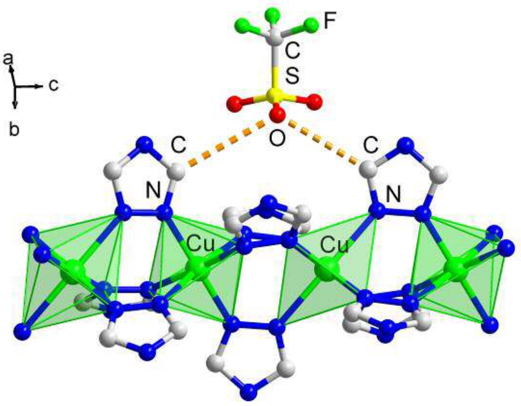

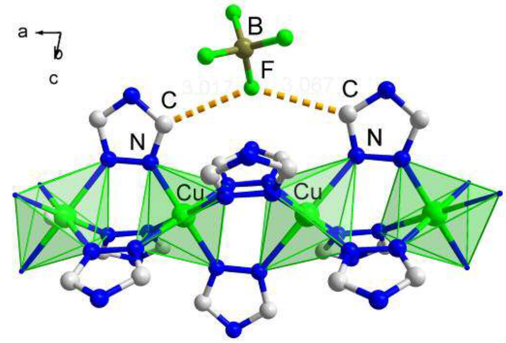

b **c**

SFigure 4. Types of the weak double hydrogen bonding CH···X···HC observed in one-dimensional polymers $[Cu(trz)_3]_\infty$, where X is: a) the oxygen atom of the water molecule; b) the oxygen atom of the triflate anion and c) the fluorine atom of the tetrafluoroborate anion. Substituents are omitted for clarity. Crystal structures were adopted from [15, 40, 41].